Dichroic Scanning Nonlinear Optical Microscope With Photodetecting Polymer Scanner and Objective Lens With External Back Focal Plane

Naitao Xu, Weiguo Liu, Jin Cheng, Menghua Wang, Bei Fang, Xin Li, and Yingshun Xu

***Abstract*—In this article authors present a prototype of a dichroic scanning nonlinear optical microscope with a photodetecting polymer Scanner and a customized objective lens with an external back focal plane. Two types of two-axis electromagnetic actuated polymer scanners are manufactured by a standard printed circuit board (PCB) fabrication process. Both scanners share the same overall dimensions of 45 mm by 45 mm. The maximum optical scan angle of a type I scanner is 13 degrees at 420 Hz by the fast axis in resonance and 4 degrees by the slow axis in the linear mode. The type II scanner shows similar performance. A scan lens as well as a tube lens in a conventional nonlinear optical microscope are replaced by placing such a polymer scanner on the external back focal plane of a customized water immersion objective lens. The objective lens has the back working distance of 6 mm, the numerical aperture of 0.7, the front working distance of 1.16 mm, a field of view of 1.67 mm in the diameter and the angle of view of +/−15 degrees. Preliminary imaging results are also presented.**

***Index Terms*—Micro and nano opto-electro-mechanical systems (MOEMS), non-linear microscopy.**

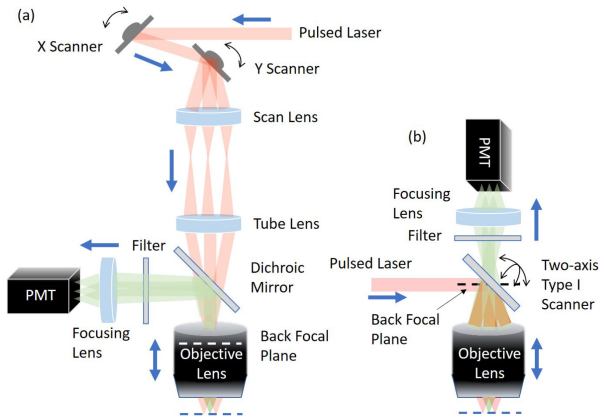

Fig. 1. Schematics of (a) a conventional NOM and (b) a DS-NOM using a type I two-axis scanner.

I. Introduction

NONLIEAR optical microscopes (NOM) including well known multiphoton microscopes (MPM) [1]–[6], harmonic generation microscopes (HGM) [7]–[10] as well as coherent anti-stokes Raman scattering (CARS) microscopic imaging modalities [11]–[15] have been widely used in subcellular resolution imaging of biological samples and live animals. In NOMs, high power ultrafast pulsed laser sources are always required to provide laser pulses with repetition rates ranging from several kilohertz to hundreds or even thousands of megahertz as well as low pulse durations down to a few femtoseconds. Based on the flying spot scanning scheme, two-dimensional or three-dimensional high-resolution images are generated by swinging a pair of scanners to move a strongly focused laser spot across image planes in the sample. High photon intensity within the tiny focal region leads to the generation of a variety of nonlinear optical signals, which enhances specific contrasts of microscopic images. In order to collect very weak and scattered nonlinear optical signals in high efficiency, a large aperture photodetector, for example, a gallium arsenide phosphide (GaAsP) photomultiplier tube (PMT) with the 5 mm sensitive area, together with a focusing lens is placed next to a main dichroic filter which locates between a tube lens and an infinity corrected objective lens for the separation of the excitation and the emission light. Since emission photons never pass the scanner, it is called the non-descanned detection (NDD) photodetection scheme.

Aiming for compact outlines, low costs as well as the large field of view (FOV) for NOMs, authors have reported a novel dichroic scanning (DS) scheme for laser scanning NOMs [16]–[18]. The relay optics consisting of a scan lens and a tube lens between the scanner and the objective lens in a conventional NOM shown in Fig. 1(a) is completely removed in a DS-NOM. Therefore, the distance between the scanner and the objective lens in a conventional NOM significantly decreases from typically around 500 mm to several millimeters in a DS-NOM. As shown in Fig. 1(b), in a DS-NOM, the main dichroic filter is integrated with a two-axis scanner and placed at the external back focal plane (BFL) of a customized objective lens. DS-NOMs eliminate constraints on the relationship of a conventional NOM where the angle of view (AOV) of an

Manuscript received August 17, 2021; accepted September 22, 2021. Date of publication September 24, 2021; date of current version October 11, 2021. This work was supported by the Science and Technology Development Fund of Tianjin Education Commission for Higher Education under Grant 2017JK232. *(Corresponding authors: Yingshun Xu; Weiguo Liu .)*

Naitao Xu, Weiguo Liu, and Jin Cheng are with the School of Optoelectronic Engineering, Xi'an Technological University, Xi'an, Shanxi 710021, China (e-mail: xunaitao_123@163.com; wgliu@163.com; cks_jcheng@163.com).

Menghua Wang is with the School of Armament Science and Technology, Xi'an Technological University, Xi'an, Shanxi 710021, China (e-mail: 15797693406@163.com).

Bei Fang, Xin Li, and Yingshun Xu are with the Department of Biomedical Engineering, School of Biomedical Engineering and Technology, Tianjin Medical University, Tianjin 300070, China (e-mail: fangbei@126.com; a2878724536@163.com; xuyingshun@tmu.edu.cn).

Digital Object Identifier 10.1109/JPHOT.2021.3115402

objective lens depends on the following equation,

$$R = \frac{\theta_{\text{objective lens}}}{\theta_{\text{scanner}}} = \frac{L_{\text{scan lens}}}{L_{\text{tubelens}}} = \frac{D_{\text{scanner}}}{D_{\text{objective lens}}}, \quad (1)$$

where stands for the focal length of a lens and indicates the laser beam diameter. Usually, the ratio R in a conventional NOM ranges from 1:4 to 1:5. In comparison with conventional NOMs equipped with Olympus objective lens of about 5.725 degrees AOV or Nikon objective lens of 7.15 degrees AOV, DS-NOMs exhibit a intrinsically large FOV and follows equations (2) and (3).

$$\theta_{objectivelens} = \theta_{scanner} \quad (2)$$

$$D_{objectivelens} = D_{scanner} \quad (3)$$

It results in a AOV of about tens of degrees in a DS-NOM. Moreover, in Fig. 1(a) and (b), positions of BFLs of objective lenses in a conventional NOM and a DS-NOM are obviously different.

In this article authors present the design, the implementation and the characterization of a prototype DS-NOM, especially critical components including two types of polymer scanners customized for DS-NOMs as well as a customized objective lens with an external BFL. The polymer material called FR4 (flame retardant) glass epoxy is a popular and versatile high-pressure thermoset plastic laminate with excellent strength to weight ratio. As a composite material, FR4 has been used to form low-cost optical scanners and NIR spectrometers [19]–[24]. In this research the type I FR4 scanner has a rotating dichroic filter rather than a common reflective mirror plate to reflect the excitation beam and allow the transmission of emission photons which are received by an external photodetector. The type II FR4 scanner performs much higher integrity by integrating a tiny silicon photodetector chip mounted by a series of thin optical filters. The embedded silicon photodetector is desired to replace the role of an external benchtop photodetector. Both two electromagnetic actuated FR4 scanners are instrumental for DS-NOMs with small dimensions as well as low costs. The design for a customized objective lens with an external BFL, the high numerical aperture (NA) and the large AOV is also presented in this article.

II. Design, Fabrication and Assembly of FR4 Scanners

A. Type I

The type I FR4 scanner is based on a two-axis gimbaled structure and actuated by the electromagnetic effect. A standard PCB fabrication process is used to manufacture the type I FR4 scanner. Copper wires are fabricated on both two sides of the PCB to form a double-layer planar coil. Two additional frames are stacked on both two sides of the main frame of the type I FR4 scanner to form a six-layer coil as the PCB layout is shown in Fig. 2(a). The type I FR4 scanner has overall dimensions of 45 mm by 45 mm and its thickness is about 0.6 mm. The cross-sectional dimension of torsional beams of a FR4 scanner is also 0.6 mm by 0.6 mm. Four pieces of N52 neodymium (NdFeB) magnets are glued on a 3D printed platform as shown in Fig 2(b). To hold a 7 mm-by-7 mm square dichroic filter, a circular aperture is drilled at the center of the mirror plate of the type I FR4 scanner. The square dichroic filter shown in Fig. 2(c) is fabricated on a quartz plate with 0.145 mm thickness. It reflects

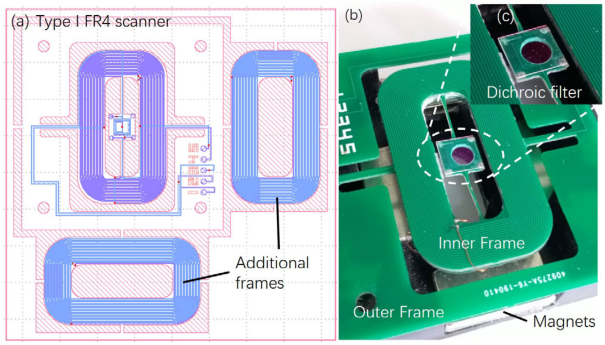

Fig. 2. (a) Layout and (b) photo of a type I FR4 scanner; (c) Closeup view of a dichroic filter.

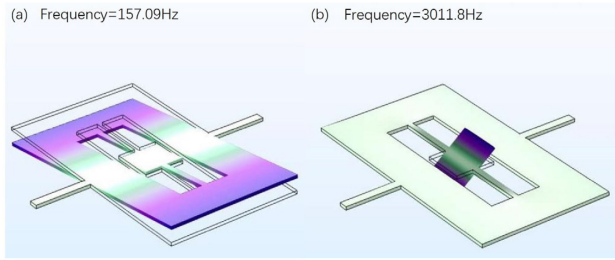

Fig. 3. Frequencies of (a) the first and (b) the ninth resonant modes of a type I FR4 scanner in the FEA simulation.

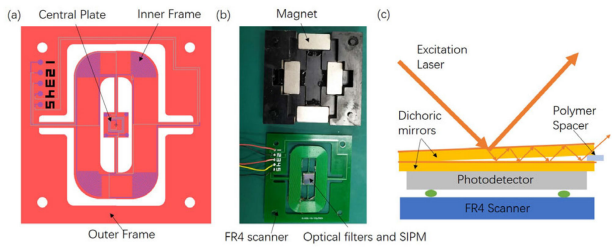

Fig. 4. (a) Layout, (b) photo and (c) cross-sectional illustration of detailed structures of a type II FR4 scanner.

near infrared (NIR) wavelengths from 780 nm to 950 nm and transmits visible wavelengths in 95%.

The Finite element analysis (FEA) of a type I FR4 scanner has been done via COMSOL. A three-dimensional model is created strictly following the dimensions of a real fabricated scanner. Specific properties of FR4 material for the FEA simulation refer to a laminated grade FR4 data sheet from Laminated Plastics [25]. Modal analysis simulation results have been shown in Fig. 3(a) and (b). The resonant mode for rotation of the mirror plate is found to be the 1st mode with the frequency of about 157 Hz while the inner frame has a rotational resonant mode in 3K Hz as the 9th mode.

B. Type II

The type II FR4 scanner shares the same layout design and the same PCB fabrication process also used in the type I FR4 scanner as seen in Fig. 4(a). It is also actuated by a group of external magnets shown in Fig. 4(b). External magnets are assembled and fixed in a 3D printed platform. At the central plate of the type II FR4 scanner from top to bottom there are two pieces of tilted dichroic filters separated by a 0.05 mm thickness polymer spacer

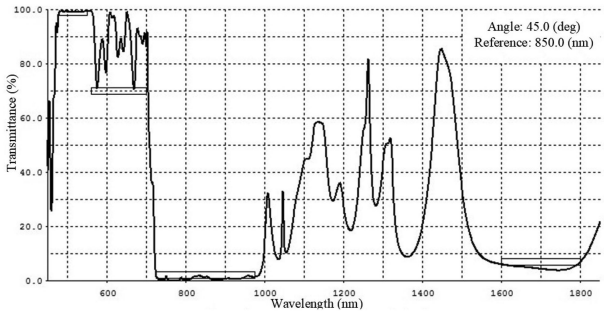

Fig. 5. Transmission curve versus wavelength of a dichroic filter in 45 degrees angle of incidence.

to introduce additional optical loss for incident excitation laser [24]. A silicon multiplier (SIPM) chip (6 mm by 6 mm sensitive area, 7 mm by 7 mm package dimensions, MICROFC-60035-SMT-TR1, ON Semiconductor, AZ, USA) is mounted on the central plate of the type II FR4 scanner in Fig. 4(c). SIPM chips feature a high internal gain up to 3x106, a low drive voltage of 3V, a photon detection efficiency (PDE) of 40% in 450 nm, which has overwhelming advantages over PMT and avalanche photodiodes (APD) in this application.

Customized dichroic filters reflect near infrared (NIR) wavelengths from 780 nm to 925 nm which covers most commonly used wavelengths for two photon fluorescence excitation and transmit emission wavelengths in 95% average transmission shown in Fig. 5. The dichroic filter performs the suppression of NIR wavelengths of about the optical density (OD) 2 at 45 degrees angle of incidence (AOI). By stacking atilt two dichroic filters, the OD value could be increased to 4. Dichroic filters are fabricated on quartz plates of the thickness of 0.145 mm and cut into 7 mm-by-7 mm squares. When the AOI changes, the transmission curve also changes. An experimental test on a similar optical filter in a variation of AOIs is reported [26]. Since wavelengths of the excitation light and the emission light in a NOM are not close to each other. Even the AOI varies from -15 degrees to $+$ 15 degrees, well designed dichroic filters are still workable.

C. Design of a Customized Objective Lens

Generally, an objective lens working in a NOM highlights its high NA for high photon collection efficiency and long working distance (WD) for sufficient working space as well penetration depth. As indicated, in a DS-NOM a scanner should swing at the BFL of the objective lens. For a high NA objective lens used in a NOM, its focal length is quite short so that the BFL of all high NA objective locates deeply within the objective lens body. it is not possible for the scanner to access the correct position. Therefore, a water immersion customized objective lens featuring its external BFL as well as the high NA and the large AOV is highly required for a DS-NOM. Design requirements of the customized objective lens are listed in Table I. The lens parameters are listed in Table II and the layout of the lens system is displayed in Fig. 6 (a) and (b). The optical design software used in this article is ZEMAX. The focal shift and the diffraction modulation transfer function (MTF) of the customized objective lens are shown in Fig. 6 (c) and (d). The MTF diagram shows that there is

TABLE I
DESIGN REQUIREMENTS FOR THE CUSTOMIZED OBJECTIVE LENS

Specification	Value
NA (water immersion)	>0.7
AOV	+/-15 degrees
Front WD	1.16mm
Back WD	6mm
FOV	1.67mm
Wavelength	920nm
Beam diameter	5mm

TABLE II
LENS DESCRIPTIONS FOR THE CUSTOMIZED OBJECTIVE LENS

Surfaces	Radius (mm)	Thickness/Distance (mm)	Optical glass
1	-3.968	4.456	H-ZLAF90
2	-6.998	0.2	
3	44.849	1.7	H-ZLAF90
4	-27.138	0.2	
5	7.733	1.7	H-ZLAF90
6	13.32	0.2	
7	3.65	2.07	H-ZLAF90
8	2.32	0.9	
9	2.85	1.663	H-ZLAF90
10	2.818		

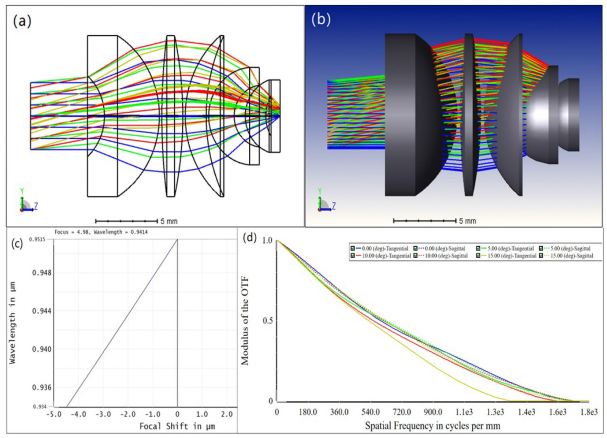

Fig. 6. (a) Structural schematics, (b) 3D shaded model, (c) focal shift diagram and (d) diffraction MTF of the customized objective lens.

excellent performance in the full FOV. The femtosecond laser (FemtoNL-920 nm-1, YSL Photonics, China) used for imaging test performs a central wavelength of 942.5177 nm. Within this wavelength range, as shown in the Fig. 6(c), the objective lens has a final focal shift of about 4.48 um. The diameter of a neuron cell is between 5 um and 150 um. Usually, the size of a neuron soma is about 20 um. Therefore, the objective lens reported in

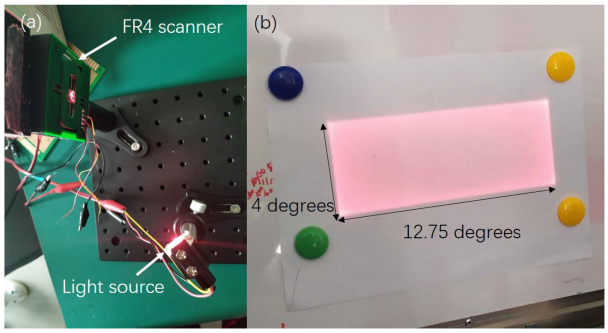

Fig. 7. (a) Experimental setup; (b) raster scan pattern.

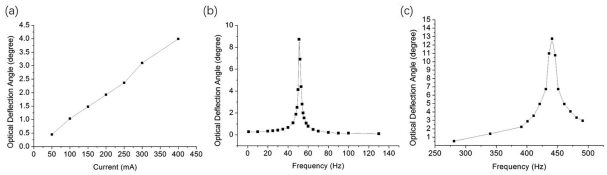

Fig. 8. (a) Current-optical deflection angle relationship of the inner frame in linear mode and frequency responses of (b) the inner frame and (c) the central plate in resonance of a Type II FR4 scanner.

the manuscript is suitable for imaging activities of neural somas rather than other smaller structures like dendrite spines of about 1 um in the diameter. The aberration such as the curvature of the field in this objective lens may not cause problems in in vivo imaging of mouse brain or bulky tissue samples like brain slices with the thickness of hundreds of micrometers.

The final design of the customized objective lens has only 5 pieces of high refractive index optical glass. All surfaces of 5 pieces of optical glass are spherical which is optimized for the fabrication and the glass material is chosen to be H-ZLAF90 (CDGM glass company Co. Ltd, China). A metallic tube, three ring spacers and a cap are precisely fabricated and used to assemble 5 pieces of optical glass together. The customized objective lens has an outer diameter of 18 mm while its length is 13 mm. Its size is obviously smaller than common objective with similar NA, magnification and WD. Due to its low fabrication cost, there are an excellent MTF and a marginal focal shift, which is acceptable for bulky sample imaging multiphoton microscopes. The optimized working wavelength of the objective lens is 920 nm for GCaMP6 calcium indicator excitation.

III. Preliminary Characterization Results

Characterizations are done by both two types of FR4 scanners. Fig. 7(a) shows the experimental setup and (b) shows a raster scan pattern generated by a FR4 scanner in its maximum deflection angles on both two axes. Measured maximum optical scan angle of a type I FR4 scanner is 13 degrees at 420 Hz by the central plate in resonance and 4 degrees by the inner frame in linear mode. The type II FR4 scanner performs its maximum optical scan angle of 12.75 degrees at 441 Hz by the central plate in resonance and 4 degrees at 400mA by the inner frame in linear mode as shown in Fig. 8(a) and (c). The Fig. 8(b) shows the resonant frequency of the inner frame is about 50 Hz.

Resolving capability of the customized objective lens is tested by imaging red polystyrene fluorescence microspheres with 920 nm two-photon excitation. Imaging samples are prepared

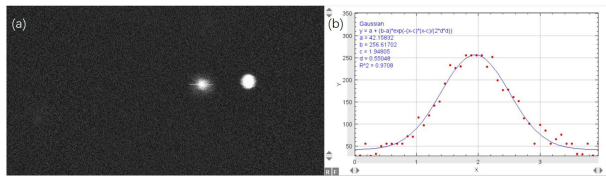

Fig. 9. (a) 8X magnified two-photon imaging of red polystyrene fluorescence microspheres of 512x273 pixels, (b) the lateral resolution of about 1.3 um in FWHM.

by dispersion of red polystyrene microspheres (1 um diameter, 1.0% w/v; BaseLine ChromTech Research Centre, China) as a scattering agent in a 0.5% agarose gel matrix (Invitrogen, Thermo Fisher Scientific, MA, USA). 119ul polystyrene microspheres were added in 1ml hot agarose gel respectively. Once the mixture reaches the room temperature, it was poured in a sample chamber and stored at 4°C keeping in dark. The proposed DS-NOM utilized with a customized objective lens as well as a type I FR4 scanner could generate 2D frames of 2048x2048 pixels, which covers an imaging area with the diameter of 1.67 mm. The required optical deflection angle for the FR4 scanner is +/−15 degrees, which equals to the AOV of the customized objective lens. However, in the current design the optical deflection angle of the FR4 scanner is still limited to less than 13 degrees in the fast axis and 4 degrees in the slow axis. It leads to 2D images of 870x273 pixels at about 1.6 Hz within a narrow rectangle area. In actual test, 2D images of 512x273 pixels are acquired. The corresponding imaging area is about 400 umx213 um while with 8X magnification the size image size of Fig. 9(a) is about 50 umx26.7 um. A customized Labview program is used to control a DAQ card (PCI-8554B, Art Technology, China) and a multifunction I/O card (PCI-8103, Art Technology, China) for digitalize signals converted by a transimpedance amplifier (TIA60, Thorlabs, NJ, USA) and manipulate the FR4 scanner. 920 nm laser pulses are generated by an ultrafast fiber laser. The laser provides 141fs laser pulses with the average power of 1watt and the repetition rate of 80M Hz. From Fig. 9(b), by Gaussian curve fitting the lateral resolution is estimated to be around 1.3 um in FWHM, which is sufficient for two-photon neural study. Due to the absence of the translation stage in the z direction, the vertical resolution is not measured this time.

IV. Discussion

Due to its intrinsic properties of glass fiber enhanced composite material, FR4 laminates' performance degradation after long time working load may appear as a material for scanner application, and this is what we need to consider in the future research. The design of FR4 scanners needs to be improved on its scan speed. Authors also attend to implement both two types of optical scanners by using microfabricated silicon MEMS technology for higher resonant frequency and larger deflection angles. Although MEMS scanners feature better performance than the FR4 scanner, the value of the FR4 dichroic scanner is the simplest and cheapest way to demonstration the concept of dichroic scanning scheme. The FR4 dichroic scanner could be used in some low-cost imaging instruments for some specific applications, for example, university education and so on.

The optical performance of the customized objective lens may attract curiosity. A typical objective lens of microscope always

TABLE III
THE COMPARISON BETWEEN THE DICHROIC SCANNING SCHEME AND MICROSCOPES REPORTED BEFORE

	Dichroic scanning scheme	Microscopes reported before
FOV	Increased	Increased
NA	unchanged	unchanged
Beam size	unchanged	Increased
Focal length	unchanged	Increased
AOV	Increased	unchanged
ObjectiveLens Dimensions	Slight increased	Apparently increased
Fabrication Cost	Low	High

has an apparently increased FOV due to its elongated focal length. In contrast, we propose a different way for achieving a large FOV. The enlarged FOV of our design mainly attributes to the increased AOV rather than the beam size as well as the focal length. Table III shows the comparison between the dichroic scanning scheme presented in this research and microscopes reported before. The pulse width of the 920 nm fiber laser used in this test is about 141fs leading to a spectral width of less than 20 nm in FWHM. Therefore, the monolithic optical design of the objective lens performs acceptable tolerance on chromatic aberrations. When working with shorter pulses which has boarder spectral width, its imaging performance may degrade significantly due to the absence of chromatic aberration compensation. It would be a technical challenge to maintain acceptable optical resolving power in such large angles by using current design. More complicated optical design is highly desired.

V. CONCLUSION

In this article authors have demonstrated a prototype of a compact DS-NOM highlighting two types of FR4 scanner as well as a customized objective lens with external BFL. A type I FR4 scanner utilizes a dichroic filter while a type II FR4 scanner rotates not only optical filters but also a tiny SIPM chip. Both FR4 scanners are electromagnetic actuated and share the same overall dimension of 45 mm by 45 mm. Maximum optical scan angle of a type I FR4 scanner is 13 degrees at 420 Hz by the fast axis in resonance and 4 degrees by the slow axis in the linear mode. The type II FR4 scanner shows similar performance but smaller deflection angle at higher resonant frequency. It is unnecessary for a DS-NOM to incorporate a scan lens and a tube lens. In a DS-NOM, a FR4 scanner scans at the back focal plane of a customized objective lens. The customized objective lens consisting of 5 pieces of high refractive index glass spherical lenses has its back WD of 6 mm away from the objective lens body. It features the high NA of 0.7, the WD of 1.16 mm, the magnification of 15x, the FOV of 1.67 mm in the diameter) and the AOV of $+/-15$ degrees. 2D two-photon images of red fluorescence microspheres are generated in 512x273 pixels. The lateral resolution is estimated to be about 1.3 um.

REFERENCES

[1] W. Denk, J. H. Strickler, and W. W. Webb, "Two-photon laser scanning fluorescence microscopy," *Science*, vol. 248, no. 4951, pp. 73–76, 1990.

[2] W. R. Zipfel, R. M. Williams, and W. W. Webb, "Nonlinear magic: Multiphoton microscopy in the biosciences," *Nature Biotechnol.*, vol. 21, no. 11, pp. 1369–1376, 2003.

[3] E. Beaurepaire, M. Oheim, and J. Mertz, "Ultra-deep two-photon fluorescence excitation in turbid media," *Opt. Commun.*, vol. 188, no. 1–4, pp. 25–29, 2001.

[4] P. Theer, M. T. Hasan, and W. Denk, "Two-photon imaging to a depth of 1000 micrometers in living brains by use of a $TiAl_2O_3$ regenerative amplifier," *Opt. Lett.*, vol. 28, no. 12, pp. 1022–1024, 2003.

[5] F. Helmchen and W. Denk, "Deep tissue two-photon microscopy," *Nature Methods*, vol. 2, pp. 932–940, 2005.

[6] M. Oheim, E. Beaurepaire, E. Chaigneau, J. Mertz, and S. Champak, "Two-photon microscopy in brain tissue: Parameters influencing the imaging depth," *J. Neurosci. Methods*, vol. 111, no. 1, pp. 29–37, 2001.

[7] X. Chen, O. Nadiarynkh, S. Plotnikov, and P. J. Campagnola, "Second harmonic generation microscopy for quantitative analysis of collagen fibrillar structure," *Nature Protoc.*, vol. 7, no. 4, pp. 654–669, 2012.

[8] R. Gauderon, P. B. Lukins, and C. J. R. Sheppard, "Optimization of second-harmonic generation microscopy," *Micron*, vol. 32, no. 7, pp. 691–700, 2001.

[9] D. S. James and P. J. Campagnola, "Recent advancements in optical harmonic generation microscopy: Applications and perspectives," *BME Front.*, vol. 2021, 2021, Art. no. 3973857.

[10] O. Masihzadeh, T. C. Lei, S. R. Domingue, M. Y. Kahook, R. A. Bartels, and D. A. Ammar, "Third harmonic generation microscopy of a mouse retina," *Mol. Vis.*, vol. 21, pp. 538–547, 2015.

[11] A. Zumbusch, G. R. Holtom, and X. S. Xie, "Three-dimensional vibrational imaging by coherent anti-stokes raman scattering," *Phys. Rev. Lett.*, vol. 82, no. 20, pp. 4142–4145, 1999.

[12] J. X. Cheng and X. Xie, "Coherent anti-stokes raman scattering microscopy: Instrumentation, theory, and applications," *J. Phys. Chem. B*, vol. 108, no. 3, pp. 827–840, 2004.

[13] B. von Vacano, T. Buckup, and M. Motzkus, "Highly sensitive single-beam heterodyne coherent anti-stokes Raman scattering," *Opt. Lett.*, vol. 31, no. 16, pp. 2495–2497, 2006.

[14] J. X. Cheng, A. Volkmer, L. D. Book, and X. S. Xie, "Multiplex coherent anti-stokes Raman scattering microspectroscopy and study of lipid vesicles," *J. Phys. Chem. B*, vol. 106, no. 34, pp. 8493–8498, 2002.

[15] H. Wang, Y. Fu, P. Zickmund, R. Shi, and J. X. Cheng, "Coherent anti-stokes Raman scattering imaging of axonal myelin in live spinal tissues," *Biophysical J.*, vol. 89, no. 1, pp. 581–591, 2005.

[16] N. Xu, W. Liu, J. Cheng, Q. Sun, W. Bao, and Y. Xu, "An all-in-one FR4 scanner assembled with optical filters and a photodetector for very low-cost multiphoton microscopes," in *Proc. Int. Conf. Opt. MEMS Nanophotonics*, 2019, pp. 70–71.

[17] J. Cheng, W. Liu, S. Zhou, N. Xu, M. Yildirim, and Y. Xu, "Ultrasmall line scan nonlinear optical microscope using 1D dichroic mems scanner and siob assembly," in *Proc. 20th Int. Conf. Solid-State Sensors, Actuators Microsystems Eurosensors XXXIII*, 2019, pp. 1564–1567.

[18] N. Xu, J. Cheng, W. Chen, Q. Sun, W. Liu, and Y. Xu, "Low cost mesoscope by a FR4 dichroic scanner and a high numerical aperture and large angle of view objective lens," in *Proc. Int. Conf. Opt. MEMS Nanophotonics*, 2019, pp. 168–169.

[19] S. Holmstrom, A. D. Yalcinkaya, S. Isikman, C. Ataman, and H. Urey, "FR-4 as a new MOEMS platform," in *Proc. IEEE/LEOS Int. Conf. Opt. MEMS Nanophotonics*, 2007, pp. 25–26.

[20] H. Urey, S. Holmstrom, and A. D. Yalcinkaya, "Electromagnetically actuated FR4 scanners," *IEEE Photon. Technol. Lett.*, vol. 20, no. 1, pp. 30–32, Jan. 2008.

[21] S. O. Isikman, R. B. Sprague, and H. Urey, "FR4 laser scanner with dynamic focus," *IEEE Photon. Technol. Lett.*, vol. 21, no. 4, pp. 233–235, Feb. 2009.

[22] S. O. Isikman *et al.*, "Advanced imaging with dynamic focus and extended depth using integrated FR4 platform," *Opt. Exp.*, vol. 17, no. 19, pp. 17179–17189, 2009.

[23] Q. Wen *et al.*, "FR4-based electromagnetic scanning micro-grating integrated with an angle sensor for a low-cost NIR micro-spectrometer," *Appl. Opt.*, vol. 58, no. 17, pp. 4642–4646, 2019.

[24] H. Lei, Q. Wen, F. Yu, Y. Zhou, and Z. Wen, "FR4-based electromagnetic scanning micromirror integrated with angle sensor," *Micromachines*, vol. 9, no. 5, 2018, Art. no. 214.

[25] [Online]. Available: https://laminatedplastics.com/fr-4.pdf

[26] Y. Xu, J. Cheng, and N. Xu, "Vibrating dichroic MEMS scanner towards ultrasmall laser scanning microscopes," in *Proc. IEEE/LEOS Int. Conf. Opt. MEMS Nanophotonics*, 2018, pp. 1–5.